Report

Current Biology

Infrasonic and Ultrasonic Hearing Evolved after the Emergence of Modern Whales

Graphical Abstract

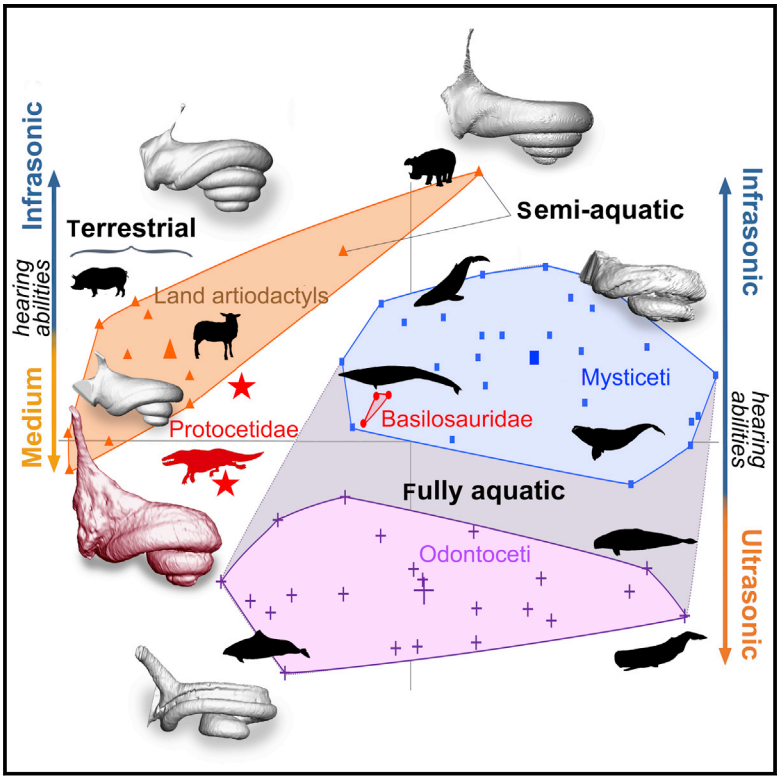

Authors

Mickaël J. Mourlam, Maeva J. Orliac

Correspondence

maeva.orliac@umontpellier.fr

In Brief

Mourlam and Orliac describe the inner ear of two partly terrestrial early whales (Protocetidae). Comparisons with other fossil and modern whales and terrestrial relatives reveal that earliest whales' hearing capacities were similar to those of their terrestrial kin and that infrasonic/ultrasonic hearing evolved after the emergence of modern whales.

Highlights

- The cochlea, headquarters of hearing, is described for two ancient protocetid whales
- These amphibious whales had hearing capacities close to those of their terrestrial kin
- Extreme hearing abilities in whales derive from a mid-frequency ancestral ear

Mourlam & Orliac, 2017, Current Biology *27*, 1776–1781
June 19, 2017
http://dx.doi.org/10.1016/j.cub.2017.04.061

CellPress

Current Biology
Report

Infrasonic and Ultrasonic Hearing Evolved after the Emergence of Modern Whales

Mickaël J. Mourlam[1] and Maeva J. Orliac[1,2,*]
[1]Institut des Sciences de l'Évolution, UMR 5554 CNRS, IRD, EPHE, Université de Montpellier, Place Eugène Bataillon, 34095 Montpellier Cedex 5, France
[2]Lead Contact
*Correspondence: maeva.orliac@umontpellier.fr
http://dx.doi.org/10.1016/j.cub.2017.04.061

SUMMARY

Mysticeti (baleen whales) and Odontoceti (toothed whales) today greatly differ in their hearing abilities: Mysticeti are presumed to be sensitive to infrasonic noises [1–3], whereas Odontoceti are sensitive to ultrasonic sounds [4–6]. Two competing hypotheses exist regarding the attainment of hearing abilities in modern whales: ancestral low-frequency sensitivity [7–13] or ancestral high-frequency sensitivity [14, 15]. The significance of these evolutionary scenarios is limited by the undersampling of both early-diverging cetaceans (archaeocetes) and terrestrial hoofed relatives of cetaceans (non-cetacean artiodactyls). Here, we document for the first time the bony labyrinth, the hollow cavity housing the hearing organ, of two species of protocetid whales from Lutetian deposits (ca. 46–43 Ma) of Kpogamé, Togo. These archaeocete cetaceans, which are transitional between terrestrial and aquatic forms, prove to be a key for determining the hearing abilities of early whales. We propose a new evolutionary picture for the early stages of this history, based on qualitative and quantitative studies of the cochlear morphology of an unparalleled sample of extant and extinct land artiodactyls and cetaceans. Contrary to the hypothesis that archaeocetes have been more sensitive to high-frequency sounds than their terrestrial ancestors [15], we demonstrate that early cetaceans presented a cochlear functional pattern close to that of their terrestrial relatives, and that specialization for infrasonic or ultrasonic hearing in Mysticeti or Odontoceti, respectively, instead only occurred in fully aquatic whales, after the emergence of Neoceti (Mysticeti+Odontoceti).

RESULTS

Morphology of the Cochlear Canal

Our study of two protocetid specimens from Kpogamé, Togo (?*Carolinacetus* sp.: isolated petrosal bone UM-KPG-M164; Protocetidae indet.: cranial fragment UM-KPG-M73; [16]) revealed that the morphology of their cochlear canal, housing the hearing organ, is unique within Cetacea and is closer to that of land artiodactyls and Mysticeti than to that of Odontoceti (Figures 1, S1, and S2; Table S1). The basal ridge, supporting the secondary bony lamina (SBL) in cetaceans [17], runs 38% (UM-KPG-M164) and 40% (UM-KPG-M73) of the cochlear canal length, respectively. These values fall within the range of Mysticeti (14%–69%; [11, 18]) and land artiodactyls (6%–71%; Data S1), whereas the extension of the SBL is greater in Odontoceti (62%–94%; [15, 19]). The coiling of the cochlear canal (UM-KPG-M73 = 2.1 turns; UM-KPG-M164 = 2.25 turns) falls within the overlapping ranges of Mysticeti (2–3.3 turns; [11]), Odontoceti (1.58–2.3 turns; [14, 20]), and land artiodactyls (e.g., *Capra hircus*, 2.25 turns; Data S1). In the two protocetid specimens from Kpogamé, the apical coiling is tight and the diameter of the cochlear canal strongly decreases toward the apex, recalling the condition of terrestrial artiodactyls. The basal ratios (height of cochlea/maximum width of basal turn; [20]) are 0.62 (UM-KPG-M164) and 0.56 (UM-KPG-M 73), values that also fall within the wide ranges of Mysticeti (0.47–0.83; [11, 18]) and land artiodactyls (0.41–0.73; Data S1). Conversely, Odontoceti display lower values (0.35–0.58; [15]). The separation between the basal turn and the second turn, or inter-turn distance, exceeds that observed in land artiodactyls (Data S1) and is similar to some Mysticeti, whereas Odontoceti display higher inter-turn distance values [15]. The cochlear canal of mammals is divided through most of its length into two Scalae: the Scala tympani (ScT) and the Scala vestibuli (ScV). Compared with other mammals, including land artiodactyls, fully aquatic cetaceans (Pelagiceti: Basilosauridae+crown Cetacea; [21]) have a ScT larger than the ScV at the basal end of the cochlea ([17]; for illustration, see also [11, 18]). The two protocetids from Kpogamé have distinct proportions: they differ from Pelagiceti in having a ScV wider than the ScT in the first half turn, and they are thus closer to the condition known in land artiodactyls (Figure S3). The two protocetids described here differ from each other in their cochlear canal dimensions and in the orientation of their cochlea inside the petrosal bone (Table S1; Figures 1A and 1E) as well as by the size of their acoustic windows, smaller in UM-KPG-M73 (Figures 1 and S1). The cochlear aqueduct, housing the perilymphatic duct, is particularly long and narrow in both specimens. Its base is much larger in UM-KPG-M164, suggesting the presence of an enlarged membranous perilymphatic duct in the latter. For additional descriptions, see Method Details in the STAR Methods.

Principal-component analysis (PCA) performed on cochlear canal measurements places the two protocetids in an intermediate position between land artiodactyls, Mysticeti, and Odontoceti, separated with no overlap (for additional information on

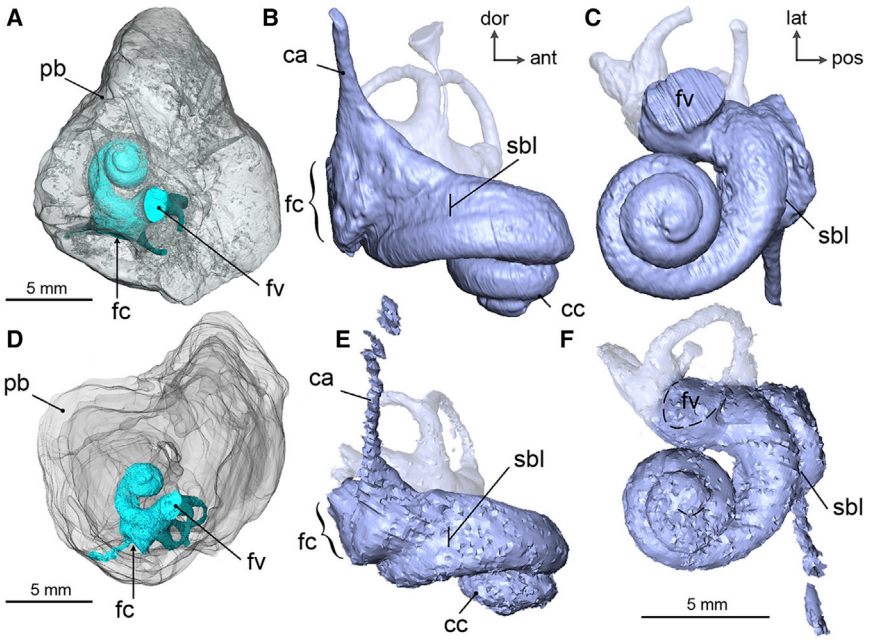

Figure 1. Digital Endocasts of the Bony Labyrinth of Protocetid Specimens from Kpogamé, Togo, with Highlighted Cochlea

(A–C) ?*Carolinacetus* sp. UM-KPG-M164.

(D–F) Protocetidae indet. UM-KPG-M73.

(A and D) In situ cochlea through a translucent rendering of the petrosal bone presented in ventral view.

(B, C, E, and F) Detail of the cochlea in medial (B and E), ventral (C), and antero-ventral (F) views. Abbreviations: ca, cochlear aqueduct; cc, cochlear canal; fc, fenestra cochleae; fv, fenestra vestibuli; pb, petrosal bone; sbl, secondary bony lamina (imprint of basal ridge). See also Figures S1, S2, and S3, and Table S1.

PCA, see Data S2 and also Method Details and Quantification and Statistical Analysis in the STAR Methods). Protocetids are located outside the morphospace of Pelagiceti, and they considerably extend the cetacean morphospace toward land artiodactyls (Figure 2). PC1 (59.45% of the variance) separates strictly terrestrial artiodactyls, which hear in air only, from Pelagiceti and hippopotamids, which are able to hear directionally underwater [14, 22]. Among the main parameters that vary along this axis are increasing widths of the basal turn, increasing length of the cochlear canal, and increasing cochlear height, which corresponds to a general increase of the size of the cochlea. Compared with terrestrial artiodactyls, aquatic and semi-aquatic taxa possess more positive scores on this axis. Odontoceti and Mysticeti are well separated on PC2 (27.13% of the variance). This axis mostly isolates high-frequency specialists, i.e., Odontoceti, from other Artiodactyla. The principal drivers of variation along this axis are the increasing number of turns and surface of the fenestra cochleae and decreasing inter-turn distance, spiral ganglion canal size, and SBL length. Increase in cochlear canal length and height (positive values on PC1) has been correlated to low-frequency hearing in cetaceans [19], as well as a high number of turns (positive values on PC2) [23]. Indeed, low-frequency specialists, also known as ''infrasonic'' artiodactyls (extant Mysticeti and *Hippopotamus amphibius*), have both positive values on PC1 and positive or slightly negative values on PC2. High-frequency hearing abilities have been correlated to increase in SBL length, inter-turn distance, and spiral ganglion canal size [17, 19, 24], parameters that have a negative contribution on PC2. Indeed, ultrasonic-hearing Odontoceti have more negative scores on this axis, whereas land artiodactyls and low-frequency or infrasonic-hearing Mysticeti have more positive scores. The same pattern is observed within land artiodactyls: taxa with a low low-frequency hearing limit have more positive scores on PC2 (e.g., *Sus scrofa* and *Bos taurus*; [25]). The two protocetids are distant on this axis (Euclidian distance = 1.21), with UM-KPG-M164 being closer to land artiodactyls and Mysticeti, and UM-KPG-M73 being closer to Odontoceti.

Evolutionary History of Characters Related to Hearing Abilities

We traced the evolutionary history of five characters related to hearing physiology traditionally used as markers of specialization toward low or high frequencies and discussed in recent works on hearing abilities of early cetaceans [11, 15]: (1) coiling of the cochlear canal [23], (2) SBL length relative to cochlear canal length [19], (3) basal ratio [17, 20], (4) diameter of the spiral ganglion canal (correlated with the number of ganglion cells [15, 24]), and (5) inter-turn distance [17]. Reconstruction of ancestral character states illustrates the mosaic pattern of character state distribution along branches within Artiodactyla and the complexity of the evolutionary history of characters related to hearing (Figure 3). The two studied protocetid petrosals show a combination close to the reconstructed ancestral state for Cetacea, with no unambiguously marked signal of increased sensitivity for low or high frequencies. The reconstructed ancestral character state combination for Neoceti implies that low-frequency sensitivity in Mysticeti and high-frequency sensitivity in Odontoceti are derived features among Cetacea. Of note, two key characters related to high-frequency hearing in cetaceans ([15]; indicated in red in Figure 3)—a large spiral ganglion (>4% of the area of the cochlear window) and a long SBL (>20% of the cochlear canal)—are also found in several terrestrial taxa (e.g., Ruminantia, *Diacodexis* or Cebochoeridae). The greatest number of character states associated with low-frequency sensitivity (indicated in blue in Figure 3) is found in Mysticeti and in modern land artiodactyls with the lowest recorded hearing range, such as Suoidea (*Sus*), Ruminantia (*Bos*), and Hippopotamoidea (*Hippopotamus*) [22, 25]. Convergent acquisitions of characters associated with low-frequency sensitivity occur in these four major artiodactyl clades.

DISCUSSION

Protocetidae are ''transitional forms'': being flesh-eaters and hunting in water, they were also most probably able to walk on the ground, coming ashore for mating, giving birth, and nursing

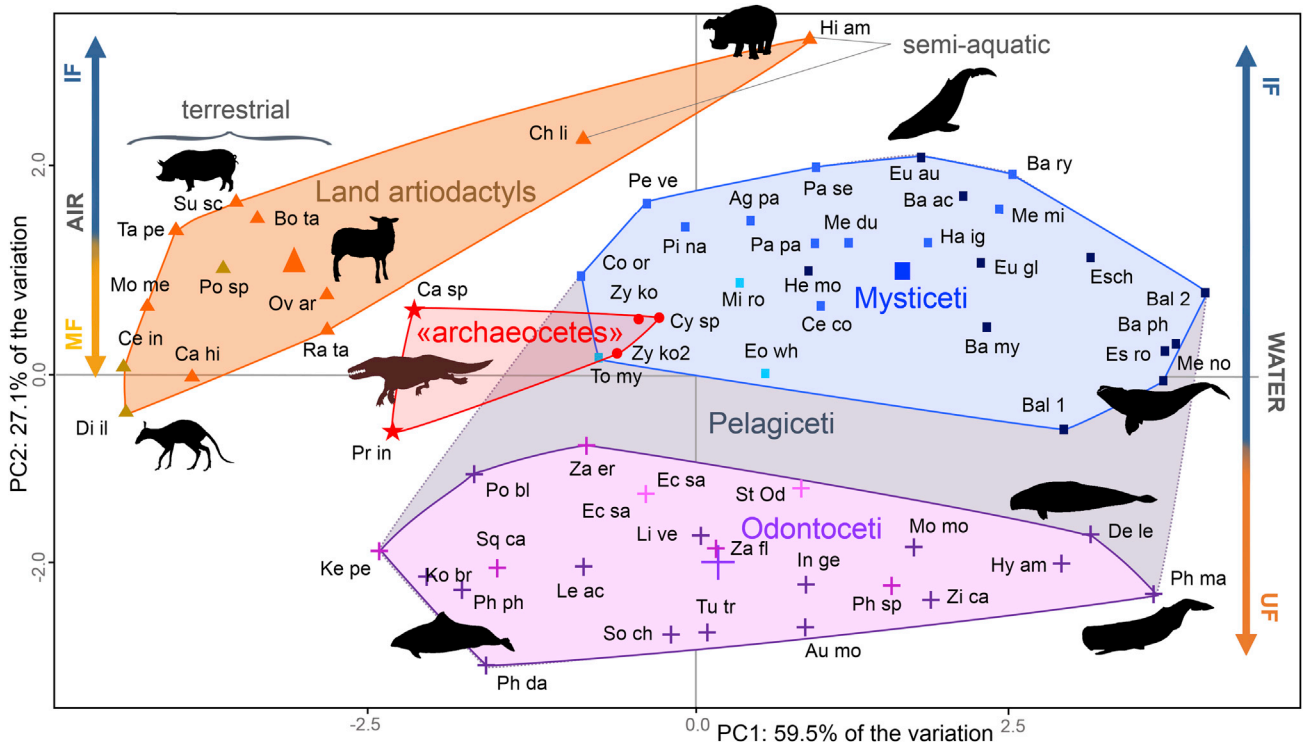

Figure 2. PCA of Nine Parameters of the Cochlea within Artiodactyla

This dataset was compiled based on the PCA of Churchill et al. [15], augmented by the two protocetids from Kpogamé, ten land artiodactyls, and data from the literature [11, 17]. Red stars represent the protocetids; red circles represent the other archaeocetes. Triangles represent extant (orange) and Paleogene (ochre) land artiodactyls. Squares represent Oligocene (cyan), Miocene (light blue), and more recent (black) mysticetes. Crosses represent Oligocene (pink), Miocene (magenta), and more recent (purple) odontocetes. The large symbols correspond to the centroid of the three main morphospaces. Abbreviations: IF, infrasonic frequencies; MF, midfrequencies; UF, ultrasonic frequencies. Abbreviations of taxa are listed in Data S1. See also Data S2.

[27–29]. It can be hypothesized that they were capable of hearing both in air and underwater [9]. The cochlear canal of the studied protocetid petrosals reflects this dual condition with both a cetacean signature (wide basal ridge supporting the SBL; high inter-turn distance) and characters and variables close to those of land artiodactyls. The cochlear canal morphology of the two protocetids studied here indicates that they were neither high-frequency specialists (ultrasonic) nor low-frequency specialists (infrasonic). The morphological distance to infrasonic taxa (i.e., Hippopotamidae and extant Mysticeti) discards the hypothesis of an increased sensitivity for low frequencies in the two protocetids of our study. Like extant mysticetes [30–32], the extant Hippopotamidae *Hippopotamus amphibius* communicates underwater at long distance using infrasonic sounds [22]. We show here that protocetids most probably did not communicate underwater over long distances using low frequencies, which is consistent with the hypothesis of a near-shore habitat [29, 33]. The two protocetids from Kpogamé differ from land artiodactyls and hippopotamids by a higher inter-turn distance, a character related to the acoustical insulation of the hearing organ [17] that could be linked with underwater hearing. Taken together, these results show that cetaceans developed strategies for hearing underwater different from those of extant amphibious hippopotamids, which is further highlighted by the deep differences in their middle ear structure (Protocetidae [8, 9, 16]; Hippopotamidae [34]).

Protocetidae are a diverse family considered as being paraphyletic [35, 36], with differences in skull shapes and limb proportions that indicate a diversity of prey preferences and locomotor abilities [29, 37, 38]. Our study shows that contemporaneous protocetids were also diversified in terms of cochlear shape and most likely had distinct hearing capacities. UM-KPG-M164, with a longer cochlea and a higher basal ratio, is morphologically closer to Mysticeti, and as such the corresponding animal might have been able to hear lower frequencies than UM-KPG-M73, which is morphologically closer to Odontoceti. Notably, UM-KPG-M164 differs from UM-KPG-M73 by the presence of a wide base of the cochlear aqueduct, a character also observed in basilosaurids [11, 15] and Mysticeti [11, 13, 18]. The cochlear aqueduct plays a role in maintaining fluid and pressure balance between the inner ear and the cerebrospinal fluid [39, 40] and might intervene in stimulating the cochlea at low frequencies ("vibroacoustic duct mechanism"; [41]).

Based on a comparison with extant Hippopotamidae, Churchill et al. [15] concluded that archaeocetes could hear higher frequencies than their terrestrial ancestors. Conversely, in including protocetids and a wider sample of land artiodactyls (further covering the diversity of crown clades among Artiodactyla), we show that early cetaceans had hearing abilities close to those of their terrestrial relatives. According to the ancestral character state distribution, in the general context of Artiodactyla, the common ancestor to crown Cetacea was not specialized toward

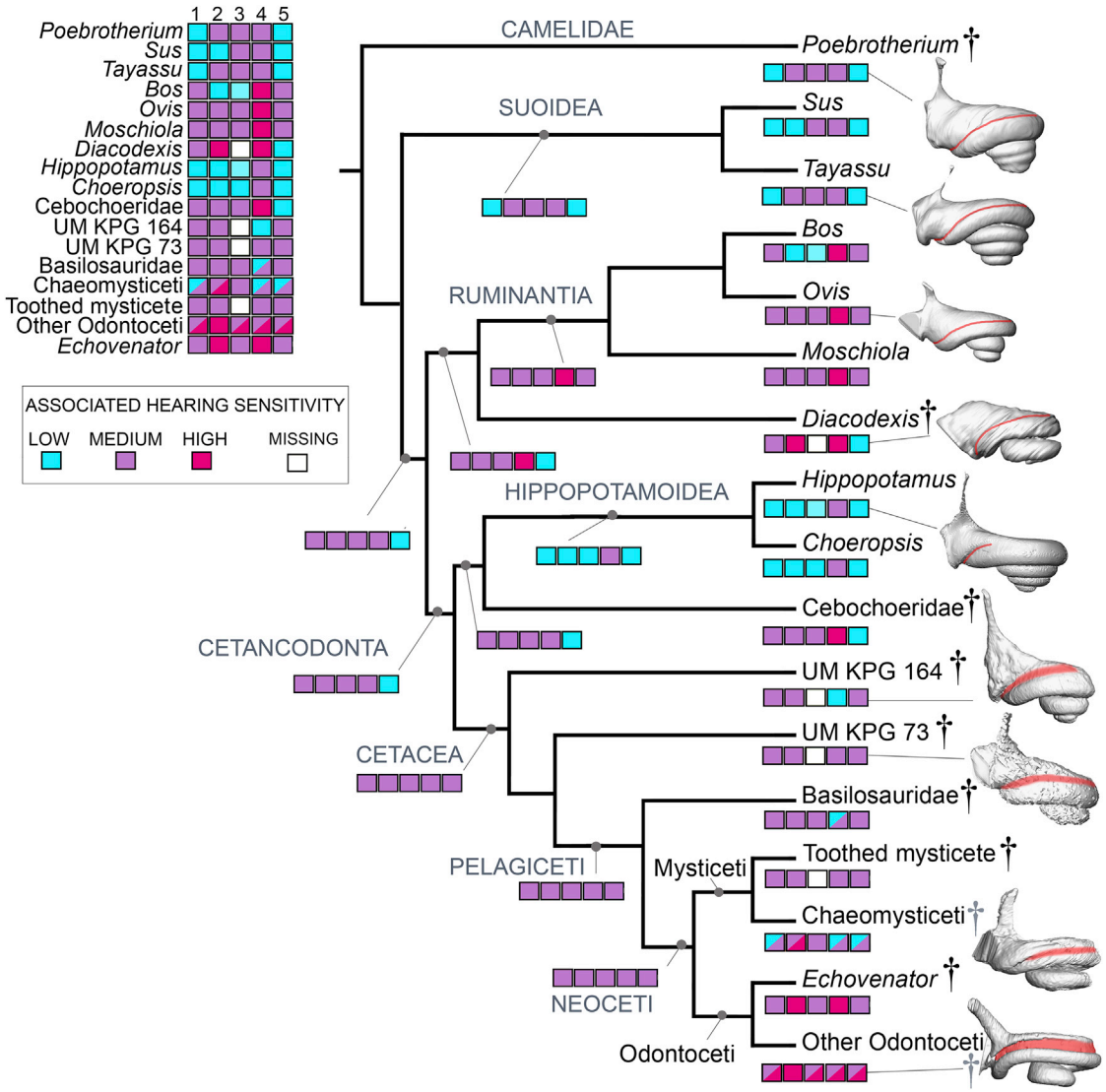

Figure 3. Distribution and Ancestral States Reconstruction of Characters Traditionally Related to Hearing Physiology within Artiodactyla

Character list: (1) number of cochlear turns: ≥3, blue; 3> and ≥2, violet; <2, pink; (2) extension of the secondary bony lamina: ≤20%, blue; 20%< and ≤61%, violet; >61%, pink; (3) spiral ganglion canal diameter expressed as a percentage of the area of the fenestra cochlearis: ≤4%, blue; 4%< and ≤8%, violet; >8%, pink; (4) basal ratio: ≥0.6, blue; 0.6> and ≥0.5, violet; <0.5, pink; and (5) inter-turn distance expressed as a percentage of basal turn width: <0.7, blue; 0.7≤ and <15, violet; ≤15, pink. Cochleae are illustrated in medial view with secondary bony lamina highlighted in red and are not to scale. Black daggers (†) indicate extinct taxa; gray daggers indicate both extinct and extant taxa. Topology is from Gatesy et al. [26] and Mourlam and Orliac [16]; "toothed mysticete" refers to the specimen ChM PV5720 [18]. For more information on tree topology, matrix, character measurements, and discretization, see Method Details in the STAR Methods. See also Data S1.

either ultrasonic or infrasonic hearing, which contrasts with previous hypotheses of low [11, 13] or high [14, 15] ancestral sensitivity in cetaceans. In contrast, Odontoceti display a highly divergent morphology from Oligocene times onward, and they have a precocious specialization toward high-frequency hearing [12]. Conversely, cochleae of basilosaurids fall within the Mysticeti morphospace, close to an unnamed toothed mysticete (ChM PV5720; [18]), highlighting that earliest fully aquatic cetaceans (Pelagiceti) were not markedly different from the earliest Mysticeti, a result further supported by the ancestral character state reconstruction. Yet, the toothed mysticete and basilosaurids are distant from recent mysticetes on the PCA (black squares in Figure 2), which suggests potential different hearing abilities. Recent baleen whales have more positive scores on PC1. The major drivers of variation on this axis can be summarized as a general increasing size of the cochlea (increasing length, width, height), and Ketten [19, 42] suggested that low-frequency cochlea in mysticetes were a consequence of increasing cochlear size. *Hippopotamus amphibius*, one of the few terrestrial artiodactyls with recorded low-frequency abilities [22], presents the largest cochlea of our terrestrial sample, further extending this supposed correlation to terrestrial taxa. In turn, earliest whales

and basilosaurids have smaller cochleae, calling their infrasonic abilities further into question (contra [13]).

Deeper in the cetacean tree, amphibious archaeocetes had hearing capabilities close to those of their terrestrial kin. It can also be inferred that the hypothetical common ancestor of Cetacea did not show any specialization for either high- or low-frequency hearing, but that it had mid-frequency hearing capabilities instead, in an optimal range to hear in both air and water [43] given its amphibious lifestyle.

The question of the ancestral hearing abilities of whales is currently highly debated. Yet, its contours are often unclear, and the answer might differ depending on how deep in the cetacean evolutionary history the debate takes place: i.e., at the Cetacea, Neoceti, or Pelagiceti level. Based on an unparalleled sample of land artiodactyls and cetaceans including non-fully aquatic taxa as a polarization criterion, we show that Protocetidae, non-fully aquatic cetaceans, lie in a morphological space between land artiodactyls, Mysticeti, and Odontoceti, and that they had hearing capacities close to those of their terrestrial kin. Based on ancestral character state reconstruction, we conclude that the extreme hearing abilities of modern whales derive from a mid-frequency ancestral ear, and that this also constituted the ancestral condition for Pelagiceti and Neoceti. Our findings show that infrasonic and ultrasonic hearing evolved in Neoceti, after the emergence of fully aquatic whales.

STAR★METHODS

Detailed methods are provided in the online version of this paper and include the following:

- KEY RESOURCES TABLE
- CONTACT FOR RESOURCE SHARING
- METHOD DETAILS
  - Acquisition of data
  - Description of the bony labyrinth of ?*Carolinacetus* sp.
  - Description of the bony labyrinth of the Protocetidae indet. γ
  - Inner ear measurements used in the analyses
  - Reconstruction of ancestral character states
- QUANTIFICATION AND STATISTICAL ANALYSIS
  - Additional information
  - Script for the analyses performed with R
  - Detailed description of the PCA results
- DATA AND SOFTWARE AVAILABILITY

SUPPLEMENTAL INFORMATION

Supplemental Information includes three figures, one table, and two data sets and can be found with this article online at http://dx.doi.org/10.1016/j.cub.2017.04.061.

AUTHOR CONTRIBUTIONS

Conceptualization: M.J.M. and M.J.O; Investigation: M.J.M. and M.J.O; Writing – Original Draft: M.J.M. and M.J.O; Supervision: M.J.O.

ACKNOWLEDGMENTS

We thank R. Araújo for assistance with the statistical treatment of data and P.-O. Antoine for comments on an early version of the manuscript. Data presented in this work were produced through the technical facilities of the Montpellier Rio Imaging platform, the LabEx CeMEB, and the AniRA-ImmOs (SFR Biosciences Gerland-Lyon) microtomography facility. This program is financially supported by the ANR program SPLASH (ANR-15-CE32-0010-01).

Received: February 28, 2017
Revised: March 31, 2017
Accepted: April 27, 2017
Published: June 8, 2017

REFERENCES

1. Houser, D.S., Helweg, D.A., and Moore, P.W.B. (2001). A Bandpass filter-bank model of auditory sensitivity in the humpback whale. Aquat. Mamm. *27*, 82–91.
2. Erbe, C. (2002). Hearing Abilities of Baleen Whales (DRDC Atlantic CR 2002-065) (Defence R&D Canada). http://cradpdf.drdc-rddc.gc.ca/PDFS/unc09/p519661.pdf.
3. Parks, S.E., Ketten, D.R., O'Malley, J.T., and Arruda, J. (2007). Anatomical predictions of hearing in the North Atlantic right whale. Anat. Rec. (Hoboken) *290*, 734–744.
4. Hemilä, S., Nummela, S., and Reuter, T. (2001). Modeling whale audiograms: effects of bone mass on high-frequency hearing. Hear. Res. *151*, 221–226.
5. Ketten, D.R. (2004). Marine mammal auditory systems: A summary of audiometric and anatomical data and implications for underwater acoustic impacts. Polarforschung *72*, 79–92.
6. Popov, V.V., and Supin, A.Y. (2007). Analysis of auditory information in the brains of cetaceans. Neurosci. Behav. Physiol. *37*, 285–291.
7. Thewissen, J.G.M., Madar, S.I., and Hussain, S.T. (1996). *Ambulocetus natans*, an Eocene cetacean (Mammalia) from Pakistan. CFS Cour. Forschungsinstitut Senckenb. *191*, 1–86.
8. Nummela, S., Thewissen, J.G.M., Bajpai, S., Hussain, S.T., and Kumar, K. (2004). Eocene evolution of whale hearing. Nature *430*, 776–778.
9. Nummela, S., Thewissen, J.G.M., Bajpai, S., Hussain, T., and Kumar, K. (2007). Sound transmission in archaic and modern whales: anatomical adaptations for underwater hearing. Anat. Rec. (Hoboken) *290*, 716–733.
10. Uhen, M.D. (2003). Form, Function, and Anatomy of *Dorudon atrox* (Mammalia, Cetacea): An Archaeocete from the Middle to Late Eocene of Egypt (Papers on Paleontology 34) (University of Michigan).
11. Ekdale, E.G., and Racicot, R.A. (2015). Anatomical evidence for low frequency sensitivity in an archaeocete whale: comparison of the inner ear of *Zygorhiza kochii* with that of crown Mysticeti. J. Anat. *226*, 22–39.
12. Park, T., Fitzgerald, E.M.G., and Evans, A.R. (2016). Ultrasonic hearing and echolocation in the earliest toothed whales. Biol. Lett. *12*, 1–4.
13. Park, T., Evans, A.R., Gallagher, S.J., and Fitzgerald, E.M.G. (2017). Low-frequency hearing preceded the evolution of giant body size and filter feeding in baleen whales. Proc. Biol. Sci. *284*, 20162528.
14. Ketten, D.R. (1992). The cetacean ear: form, frequency, and evolution. In Marine Mammal Sensory Systems, J.A. Thomas, R.A. Kastelein, and A.Y. Supin, eds. (New York: Plenum Press), pp. 53–75.
15. Churchill, M., Martinez-Caceres, M., de Muizon, C., Mnieckowski, J., and Geisler, J.H. (2016). The Origin of High-Frequency Hearing in Whales. Curr. Biol. *26*, 2144–2149.
16. Mourlam, M.J., and Orliac, M.J. (2017). Protocetid (Cetacea, Artiodactyla) bullae and petrosals from the Middle Eocene locality of Kpogamé, Togo: new insights into the early history of cetacean hearing. J. Syst. Palaeontol. Published online May 30, 2017. http://dx.doi.org/10.1080/14772019.2017.1328378.
17. Fleischer, G. (1976). Hearing in extinct cetaceans as determined by cochlear structure. J. Paleontol. *50*, 133–152.
18. Ekdale, E.G. (2016). Morphological variation among the inner ears of extinct and extant baleen whales (Cetacea: Mysticeti). J. Morphol. *277*, 1599–1615.

19. Ketten, D.R. (1992). The marine mammal ear: specializations for aquatic audition and echolocation. In The Evolutionary Biology of Hearing, D.B. Webster, A.N. Popper, and R.R. Fay, eds. (New York: Springer-Verlag), pp. 717–750.
20. Ketten, D.R., and Wartzok, D. (1990). Three-dimensional reconstructions of the dolphin ear. In Sensory Abilities of Cetaceans: Laboratory and Field Evidence, J.A. Thomas, and R.A. Kastelein, eds. (New York: Plenum Press), pp. 81–105.
21. Uhen, M.D. (2008). New protocetid whales from Alabama and Mississippi, and a new cetacean clade, Pelagiceti. J. Vertebr. Paleontol. *28*, 589–593.
22. Barklow, W.E. (2004). Amphibious communication with sound in hippos, *Hippopotamus amphibius*. Anim. Behav. *68*, 1125–1132.
23. West, C.D. (1985). The relationship of the spiral turns of the cochlea and the length of the basilar membrane to the range of audible frequencies in ground dwelling mammals. J. Acoust. Soc. Am. *77*, 1091–1101.
24. Luo, Z.-X., and Marsh, K. (1996). Petrosal (periotic) and inner ear of a Pliocene Kogiine whale (Kogiinae, Odontoceti). Implications on relationships and hearing evolution of toothed whales. J. Vertebr. Paleontol. *16*, 328–348.
25. Heffner, R.S., and Heffner, H.E. (1990). Hearing in domestic pigs (*Sus scrofa*) and goats (*Capra hircus*). Hear. Res. *48*, 231–240.
26. Gatesy, J., Geisler, J.H., Chang, J., Buell, C., Berta, A., Meredith, R.W., Springer, M.S., and McGowen, M.R. (2013). A phylogenetic blueprint for a modern whale. Mol. Phylogenet. Evol. *66*, 479–506.
27. Gingerich, P.D., Raza, S.M., Arif, M., Anwar, M., and Zhou, X. (1994). New whale from the Eocene of Pakistan and the origin of cetacean swimming. Nature *368*, 844–847.
28. Gingerich, P.D., Ul-Haq, M., von Koenigswald, W., Sanders, W.J., Smith, B.H., and Zalmout, I.S. (2009). New protocetid whale from the middle eocene of pakistan: birth on land, precocial development, and sexual dimorphism. PLoS ONE *4*, e4366.
29. Thewissen, J.G.M., Cooper, L.N., George, J.C., and Bajpai, S. (2009). From land to water: the origin of whales, dolphins and porpoises. Evol. Educ. Outreach *2*, 272–288.
30. Payne, R., and Webb, D. (1971). Orientation by means of long range acoustic signaling in baleen whales. Ann. N Y Acad. Sci. *188*, 110–141.
31. Spiesberger, J.L., and Fristrup, K.M. (1990). Passive localizations of calling animals and sensing of their acoustic environment using acoustic tomography. Am. Nat. *135*, 107–153.
32. Tyack, P.L. (1999). Communication and cognition. In Biology of Marine Mammals, J.E. Reynolds, II, and S.A. Rommel, eds. (Washington, DC: Smithsonian Institution Press), pp. 287–323.
33. Williams, E.M. (1998). Synopsis of the earliest cetaceans Pakicetidae, Ambulocetidae, Remingtonocetidae, and Protocetidae. In The Emergence of Whales, J.G.M. Thewissen, ed. (New York: Plenum Press), pp. 1–28.
34. Orliac, M.J., Guy, F., and Lebrun, R. (2014). Osteological connections of the petrosal bone of the extant Hippopotamidae *Hippopotamus amphibius* and *Choeropsis liberiensis*. MorphoMuseuM *1*, e1.
35. Geisler, J.H., Sanders, A.E., and Luo, Z.-X. (2005). A new protocetid whale (Cetacea: Archaeoceti) from the Late Middle Eocene of South Carolina. Am. Mus. Novit. *3480*, 1–65.
36. Gol'din, P., and Zvonok, E. (2013). *Basilotritus uheni*, a new cetacean (Cetacea, Basilosauridae) from the Late Middle Eocene of Eastern Europe. J. Paleontol. *87*, 254–268.
37. Gingerich, P.D., Zalmout, I.S., Ul-Haq, M., and Akram Bhatti, M. (2005). *Makaracetus bidens*, a new protocetid archaeocete (Mammalia, Cetacea) from the early middle Eocene of Balochistan (Pakistan). Contrib. Mus. Paleontol. Univ. Mich. *31*, 197–210.
38. Bianucci, G., and Gingerich, P.D. (2011). *Aegyptocetus tarfa*, n. gen. et sp. (Mammalia, Cetacea), from the middle Eocene of Egypt: Clynorhynchy, olfaction, and hearing in protocetid whale. J. Vertebr. Paleontol. *31*, 1173–1188.
39. Carlborg, B., Densert, B., and Densert, O. (1982). Functional patency of the cochlear aqueduct. Ann. Otol. Rhinol. Laryngol. *91*, 209–215.
40. Hofman, R., Segenhout, J.M., Albers, F.W.J., and Wit, H.P. (2005). The relationship of the round window membrane to the cochlear aqueduct shown in three-dimensional imaging. Hear. Res. *209*, 19–23.
41. March, D., Brown, D., Gray, R., Curthoys, I., Wong, C., and Higgins, D.P. (2016). Auditory anatomy of beaked whales and other odontocetes: Potential for cochlear stimulation via a "vibroacoustic duct mechanism." Mar. Mamm. Sci. *32*, 552–567.
42. Ketten, D.R. (2000). Cetacean ears. In Hearing by whales and dolphins, W.W.L. Au, A.N. Popper, and R.R. Fay, eds. (New York: Springer), pp. 43–108.
43. Møhl, B. (1968). Auditory sensitivity of the common seal in air and water. J. Aud. Res. *8*, 27–38.
44. Orliac, M.J., Benoit, J., and O'Leary, M.A. (2012). The inner ear of Diacodexis, the oldest artiodactyl mammal. J. Anat. *221*, 417–426.
46. Lebrun, R., and Orliac, M.J. (2016). MorphoMuseuM: an online platform for publication and storage of virtual specimens. Paleontol. Soc. Pap. *22*, 183–195.
47. Maddison, W.P., and Maddison, D.R. (2017). Mesquite: a modular system for evolutionary analysis. http://mesquiteproject.org.
48. R Core Development Team (2015). R: A language and environment for statistical computing. https://www.r-project.org/.
49. Lê, S., Josse, J., and Husson, F. (2008). FactoMineR: An {R} package for multivariate analysis. J. Stat. Softw. *25*, 1–18.
50. Josse, J., and Husson, F. (2016). missMDA: A package for handling missing values in multivariate data analysis. J. Stat. Softw. *70*, 1–31.
51. Komsta, L. (2011). Outliers: Tests for outliers. http://cran.r-project.org/package=outliers.
52. Gingerich, P.D., and Cappetta, H. (2014). A new archaeocete and other marine mammals (Cetacea and Sirenia) from lower middle Eocene phosphate deposits of Togo. J. Paleontol. *88*, 109–129.
53. Geisler, J.H., and Luo, Z.-X. (1996). The petrosal and inner ear of *Herpetocetus* sp. (Mammalia Cetacea) and their implications for the phylogeny and hearing of archaic Mysticetes. J. Paleontol. *70*, 1045–1066.
54. Ekdale, E.G., and Rowe, T. (2011). Morphology and variation within the bony labyrinth of zhelestids (Mammalia, Eutheria) and other therian mammals. J. Vertebr. Paleontol. *31*, 658–675.
55. Ekdale, E.G. (2013). Comparative anatomy of the bony labyrinth (inner ear) of placental mammals. PLoS ONE *8*, e66624.
56. Flydal, K., Hermansen, A., Enger, P.S., and Reimers, E. (2001). Hearing in reindeer (*Rangifer tarandus*). J. Comp. Physiol. A Neuroethol. Sens. Neural Behav. Physiol. *187*, 265–269.
57. Wartzok, D., and Ketten, D.R. (1999). Marine mammal sensory systems. In Biology of Marine Mammals, J.E. Reynolds, II, and S.A. Rommel, eds. (Washington, DC: Smithsonian Institution Press), pp. 117–136.
58. Mooney, T.A., Yang, W.C., Yu, H.-Y., Ketten, D.R., and Jen, I.-F. (2015). Hearing abilities and sound reception of broadband sounds in an adult Risso's dolphin (*Grampus griseus*). J. Comp. Physiol. A Neuroethol. Sens. Neural Behav. Physiol. *201*, 751–761.
59. Grubbs, F.E. (1950). Sample criteria for testing outlying observations. Ann. Math. Stat. *21*, 27–58.
60. Smith, A.S., and Araújo, R. (2017). *Thaumatodracon wiedenrothi*, a morphometrically and stratigraphically intermediate new rhomaleosaurid plesiosaurian from the Lower Jurassic (Sinemurian) of Lyme Regis. Palaeontogr. Abt. A Palaeozool. Stratigr. *308*, 89–125.
61. Mahalanobis, P.C. (1936). On the generalized distance in statistics. Proc. Natl. Inst. Sci. India *2*, 49–55.

STAR★METHODS

KEY RESOURCES TABLE

RESOURCE	SOURCE	IDENTIFIER
Taxa		
?*Carolinacetus*	This paper	UM-KPG-M 164
cf. *Cynthiacetus*	[15]	CCNHM 167
Protocetid indet. γ	This paper	UM-KPG-M 73
Zygorhiza kochii	[11]	USNM PAL 214433
Zygorhiza kochii	[15]	USNM 4748
Bos taurus	This paper	UPPal ART-8-055
Capra hircus	This paper	UM-543N
Cebochoeridae indet.	This paper	UM-SNB-2257
Choeropsis liberiensis	This paper	UPPal-M09-5-005a
Diacodexis ilicis	[44], this paper	AMNH VP 16141
Hippopotamus amphibius	This paper	UM-N179
Moschiola meminna	This paper	UM-58V
Ovis aries	This paper	UM-785N
Poebrotherium	This paper	AMNH not numbered
Rangifer tarandus	This paper	UPPal ART-12-020
Sus scrofa	This paper	UM-784N
Tayassu pecari	This paper	UM-N-03
"*Balaenoptera*" *ryani*	[18]	CAS 1733
"*Megaptera*" *miocaena*	[11]	USNM V10300
Aglaocetus patulus	[18]	USNM V 23690
Balaena mysticetus	[11]	LACM 97312
Balaenoptera acutorostrata	[11]	SDNHM 23642
Balaenoptera physalus	[15]	MNHN AZ.MC.1989.403
Balaenopteridae	[11]	SDSNH 83695
Balaenopteridae	[11]	TMM 42958-35
Cephalotropis coronatus	[18]	CMM-V-3636
Cophocetus oregonensis	[18]	UO F36450
Eomysticetus whitmorei	[18]	ChM PV4253
Eschrichtiidae	[11]	SDSNH 65021
Eschrichtius robustus	[11]	SDNHM 24316
Eubalaena australis	[15]	MNHN AZ.MC 1877-93
Eubalaena glacialis	[11]	LACM 54763
Halicetus ignotus	[18]	USNM V23636
Herpetocetus morrowi	[18]	SDSNH 63690
Megaptera novaeangliae	[11]	HSU VM2776
Metopocetus durinasus	[18]	USNM V8518
Micromysticetus rothauseni	[18]	ChM PV7225
Parietobalaena cf. *P. securis*	[18]	SDSNH 61095
Parietobalaena palmeri	[18]	USNM 517872
Peripolocetus vexillifer	[18]	SDSNH 53999
Piscobalaena nana	[15]	MNHN F.SAS 892
Toothed mysticete	[18]	ChM PV5720
Aulophyseter morricei	[18]	SDSNH 55015
Delphinapterus leucas	[15]	MNHN AZ.MC.A3548

(*Continued on next page*)

Continued		
RESOURCE	SOURCE	IDENTIFIER
Echovenator sandersi	[15]	GSM 1098
Hyperoodon ampullatus	[15]	MNHN 1913-286
Inia geoffrensis	[15]	MNHN uncatalogued
Kentriodon pernix	[15]	USNM 8060
Kogia breviceps	[15]	MNHN 1877-277
Leucopleurus acutus	[15]	AMNH 143513
Lipotes vexillifer	[15]	AMNH 57333
Monodon monoceros	[15]	AMNH 254554
Phocageneus sp.	[15]	USNM 182942
Phocoena phocoena	[15]	MNHN AZ.MC.A3548
Phocoenoides dalli	[15]	MNHN 1992-47
Physeter macrocephalus	[15]	MNHN 1981-36
Pontoporia blainvillei	[15]	AMNH 254554
Sousa chinensis	[15]	MNHN 1993-88
Squalodon calvertensis	[15]	USNM 10484
Stem odontocete	[18]	ChM PV2776
Tursiops truncates	[15]	MNHN AZ.MC.1903-201
Zarhachis flagellator	[15]	USNM 10484
Zarhinocetus errabundus	[18]	SDSNH 86299
Ziphius cavirostris	[15]	MNHN 1902-218
Software and Algorithms		
AVIZO 9.0	FEI	https://www.fei.com/software/amira-avizo/
ISE-MeshTools 1.3	[46]	http://morphomuseum.com/meshtools
Mesquite 3.2	[47]	http://mesquiteproject.org
R 3.3.0	[48]	https://www.r-project.org/
FactoMineR (R package)	[49]	https://cran.r-project.org/web/packages/FactoMineR/index.html
missMDA (R package)	[50]	https://cran.r-project.org/web/packages/missMDA/index.html
outliers (R package)	[51]	http://cran.r-project.org/package=outliers
Other		
?*Carolinacetus* (3D model)	MorphoMuseuM.com	MorphoMuseuM: M3#149_UMKPG-M164 (https://doi.org/10.18563/m3.sf.149)
Protocetid indet. γ (3D model)	MorphoMuseuM.com	MorphoMuseuM: M3#150_UMKPG-M73 (https://doi.org/10.18563/m3.sf.150)
Datasets used for PCA and for the reconstruction of ancestral character states	This paper	Data S1

CONTACT FOR RESOURCE SHARING

Further information and requests for resources should be directed to, and will be fulfilled by, the corresponding author Maeva J. Orliac (maeva.orliac@umontpellier.fr).

METHOD DETAILS

Acquisition of data

The two protocetid specimens were collected in the same bone bed at Kpogamé, Togo; the fragmentary cranium UM-KPG-M73 was originally described by Gingerich and Cappetta [52]. The two specimens described here were subsequently referred to ?*Carolinacetus* sp. (UM-KPG-M164) and Protocetidae indet. γ (UM-KPG-M73) by Mourlam and Orliac [16]. The isolated petrosal UM-KPG-M164 was scanned with a resolution of 36 μm using the Skyscan/1076/ in-vivo CT scanner at the MRI CT-scan facility (Institut des Sciences de l'Évolution, Université de Montpellier, France). The fragmentary cranium UM-KPG-M73 was scanned at the AniRA-ImmOs (SFR Biosciences Gerland-Lyon) microtomography facility using a General Electric Phoenix Nanotom S with a resolution of 70 μm. We extracted virtually the endocast of the bony labyrinth slice by slice manually using the segmentation tools of AVIZO 9.0 (FEI). The

3D models are available at MorphoMuseuM.com (M3#149_UMKPG-M164, M3#150_UMKPG-M73). Detailed descriptions of the petrosal bones of ?*Carolinacetus* sp. and Protocetidae indeterminate (morphotype γ) are available in Mourlam and Orliac [16].

Description of the bony labyrinth of ?*Carolinacetus* sp.

Cast of the bony labyrinth

The bony labyrinth fills a small part of the petrosal volume (Figure 1): the cochlea occupies most of the volume of the pars cochlearis, but the semicircular canals spread on a very small part of the mastoid region of the pars canalicularis. Measurements of the 3D reconstruction of the labyrinth endocasts of UM-KPG-M 164 are provided in Table S1. Part of the lateral semicircular canal cannot be reconstructed because of a breakage of the petrosal and thinnest structures of the cochlea area, such as the secondary bony lamina and the wall that separates the successive turns of the cochlear canal are only partially preserved. The modiolus, the central bony axis of the cochlea, is not preserved and the primary bony lamina cannot be observed.

Cochlear canal

The cochlea contributes 73.6% of the total volume of the bony labyrinth (Table S1). The coiling of the cochlear canal completes 2.25 turns (rotation of 810°) and the basal ratio equals 0.62. The axial pitch of the cochlea equals 2.33, and its slope equals 0.075. The diameter of the cochlear canal strongly decreases toward the apex, and the height of the external wall of the second turn is half that of the basal turn. The basal turn is globose with an oval cross section. The second turn is separated from the basal turn by a thin layer of bone. The bony layer between the second and third turns is not preserved but must have been particularly thin, thinner than that separating the second turn from the basal turn. The secondary bony lamina, projecting from the outer wall of the cochlear canal, is partly preserved but its bony support, the basal ridge, leaves a wide and shallow groove on the cochlear cast that vanishes very shortly around 180° (Figures S1A, S2A-C). The extension of the basal ridge covers around 38% of the cochlear canal length. The cochlear aqueduct (housing the perilymphatic duct) is long and round in cross section. It is wide at its base (Lbase = 4.62 mm; Wbase = 2.07 mm), but its diameter is rather thin on most of its length (diameter = 0.6 mm). It emerges at the dorsomedial edge of the fenestra cochleae and projects posteromedially (Figures S1D and S1E). The basal turn of the cochlear canal is enlarged at the level of the cochlear aqueduct. In section, the cochlear canal shows a Scala vestibuli wider than the Scala tympani in the first half of the basal turn (Figure S3).

Vestibular system

The distinction between the spherical and elliptical recesses is subtle, the swelling of the small elliptical recess is visible in dorsal and anterior views of the labyrinth and separated from the slightly more important bulge of the spherical recess by a slight depression visible in anterior view (Figure S1). The elliptical recess is straight and elongated (dorsal view). The vestibular aqueduct (housing the endolymphatic duct) exits the vestibule anterior to the basis of the short common crus and raises parallel to it. The anterior semicircular canal (ASC) shows the greatest extent dorsally while the lateral semicircular canal (LSC), although broken, appears to have the greatest radius and to be the longest of the three semicircular canals (Table S1). The posterior semicircular canal (PSC) is the smallest. The posterior limb of the LSC does not empty into the vestibule via its own foramen, it fuses with the PSC shortly before the posterior ampulla in a very short secondary common crus (Figure S1) in which the course of both canal can be distinguished. The ASC and PSC are straight along their course and lie in a single plane (Figure S1). The LSC seems to be slightly sigmoid, but its course is interrupted by a breakage of the petrosal bone. The angle between the ASC and LSC is the smallest, and the angle between the ASC and PSC is the widest (Table S1). The three ampullae are teardrop in shape. The posterior ampulla attaches to the vestibule slightly below the level of the LSC horizontal plane, whereas the anterior ampulla is located slightly above this plane (Figure S1). The long axis of the short common crus points dorsally to the posterior direction.

Description of the bony labyrinth of the Protocetidae indet. γ

Bony labyrinth

The quality of the model of the bony labyrinth of the specimen UM-KPG-M 73 is limited due to the rather low contrast of the CT slices resulting from high density of the bone and matrix. Measurements of the cast of the bony labyrinth are provided in Table S1 and Data S1. Part of the posterior semicircular canal could not be reconstructed because of a breakage of the petrosal. Like in UM-KPG-M 164, the bony labyrinth fills a small part of the petrosal volume only (Figure 1).

Cochlear canal

Visualization of the cochlear canal through a translucent rendering of the petrosal bone shows that the orientation of the cochlea of UM-KPG-M 73 differs from that of UM-KPG-M 164 referred to ?*Carolinacetus* by a more anterior orientation of the apex. The cochlea contributes 69.6% of the total volume of the bony labyrinth (Table S1). The coiling of the cochlear canal completes 2.1 turns (rotation of 765°) which is little bit less than in UM-KPG-M 164. The basal ratio equals 0.56, a little lower value than that calculated for UM-KPG-M 164. The axial pitch of the cochlea equals 2.76, and the slope 0.103. Taken altogether these values slightly differ from those of UM-KPG-M 164 which presents a "higher cochlea" with higher turns. Like in UM-KPG-M 164, the diameter of the cochlear canal of UM-KPG-M 73 strongly decreases toward the apex. The basal turn is globose and is oval in cross section, and the second turn is separated from the basal turn by a thin layer of bone. The basal ridge supporting the secondary bony lamina is visible on only half of the first turn of the cochlear canal cast (Figures S1F, S2D-S2F). It runs on 39.6% of the cochlear canal length and leaves a wide and shallow groove on the cast of the cochlear canal. The cochlear aqueduct is particularly long and thin (diameter = 0.5 mm). Unfortunately, the total length of the cochlear aqueduct of UM-KPG-M 164 could not be determined because of breakage of the petrosal and comparison are therefore impossible. However, the base of the cochlear aqueduct of UM-KPG-M 73 is much

narrower than that of UM-KPG-M 164 (Lbase = 2.25 mm; Wbase = 1.35 mm) (Figure S1D versus S1I). In section, the cochlear canal shows a Scala vestibuli wider than the Scala tympani in the first half of the basal turn (Figures S2F, S3).

Vestibular system

The distinction between the spherical and elliptical recesses is unclear due to the limited quality of the reconstruction. Like in UM-KPG-M 164, the elliptical recess is straight and elongated (dorsal view). The available reconstruction of the vestibular aqueduct is too partial to allow proper description. In UM-KPG-M 73, like in UM-KPG-M 164, the ASC shows the greatest extent dorsally and the LSC has the greatest radius (Table S1). However, contrary to UM-KPG-M 164, the ASC is also the longest of the three semicircular canals (and not the LSC). The ASC of UM-KPG-M 73 has a more circular profile. The PSC is the shortest semicircular canal. Like in UM-KPG-M 164, there is a very short secondary common crus (Figure S1). The ASC is straight along its course and the LSC is only slightly sigmoid. The angles between the semicircular canals are slightly more open in UM-KPG-M 73 (Table S1). The anterior and lateral ampullae are slightly less inflated. Like in UM-KPG-M 164, the long axis of the short common crus points dorsally to the posterior direction.

Inner ear measurements used in the analyses

Nine cochlear measurements related to hearing physiology have been selected in PCA and are used, mostly through ratios in the ancestral character sate reconstruction section. The length of the cochlear canal has been measured following the protocol of West [23] using the virtual line passing in the center of the cochlear lumen. The number of cochlear turns was determined according to the protocol described in Geisler and Luo [53], also used in Ekdale and Rowe [54] and Ekdale [55]. The basal ratio corresponds to: height of cochlea (Ch) /maximum width of basal turn (Cw) [20]. The width W2 corresponds to the shorter diameter of the basal turn, perpendicular to Cw, as originally defined by Churchill et al. [15]. The inter-turn distance, ITD, corresponds to the thickness of the bony wall separating the first turn from the second turn at the proximal end of the basal turn, following Ekdale and Racicot [11]. The diameter of the spiral canal was measured in the first quarter of the basal turn. Linear measurements were taken using the 3D measurement tool of AVIZO 9.0 (FEI) and the curve info option of ISE-MeshTools [46]. Volumes of the bony labyrinth were calculated including the endolymphatic and perilymphatic ducts, with AVIZO 9.0.

Reconstruction of ancestral character states

We mapped the character states of five characters related to hearing physiology traditionally used as markers of specialization toward low or high frequency and discussed in recent works on hearing abilities of early cetaceans [11, 15]. All these characters are ratios of measurements which allows to minimize the impact of the size of the specimen. Discretization of these continuous variables follows the literature when possible. Otherwise, character states have been designed in order to highlight extreme values. Corresponding matrix is provided in Figure 3 and below. We followed the evolutionary history of these five characters using the Trace Character History facility of Mesquite 3.2 [47] with parsimony ancestral state option. We used phylogenetic relationships proposed by Gatesy et al. [26] and Mourlam and Orliac [16].

Character 1: Coiling of the cochlea

A greater number of coils reflects lower frequency sensitivity [23].

Character states: $\geq$ 3, blue; 3 > and $\geq$ 2, violet; < 2, pink

Character 2: Extension of the secondary bony lamina

The more the SBL is extended, highest the sensibility to high frequencies. In reverse, a weak extension of the SBL over the basilar membrane (or cochlear canal) may correlate with low-frequency limits [19]. The extension of the SBL is here expressed as a percentage of the cochlear canal length. Bounds follow Churchill et al. [15, Figure 3] with "long" SBL > 20% and "very long" SBL > 61%.

Character states: $\leq$ 20%, blue; 20% < and $\leq$ 61%, violet; > 61%, pink

Mysticeti present the tree character states, they have been considered as ancestrally violet based on character reconstruction state after the topology of Ekdale [18]. The character state $\leq$ 20%, observed in *Eubalaena glacialis* has been considered as derived within Mysticeti according to the cladogram provided by Ekdale [18, Figure 1] and was not indicated on Figure 3 in order to facilitate reading.

Character 3: Spiral ganglion canal diameter

Larger spiral ganglion canal in the first part of the of the basal turn, where high-frequency sounds are detected, may correlate with more ganglion cells and increased innervation and signal processing capability [15, 24]. The diameter of the spiral ganglion is here expressed as a percentage of the area of the fenestra cochlearis following Churchill et al. [15, Figure 3] with "large" spiral ganglion canal > 4% and "huge" ganglion canal > 8%.

Character states: $\leq$ 4%, blue; 4% < and $\leq$ 8%, violet; > 8%, pink.

The character state $\leq$ 4%, observed in *Delphinapterus leucas* has been considered as derived within Odontoceti and was not indicated on Figure 3 in order to facilitate reading.

Character 4: Basal ratio of the cochlea

The basal ratio reflects both expansion of the basal turn, where high-frequency sounds are detected, and the number of coils of the cochlea. A high basal ratio correlates for ultrasonic hearing in cetaceans [20]. Basal ratio inferior to 0.6 is considered by Churchill et al. [15, Figure 3] as a hallmark of ultrasonic hearing in Cetacea. We distinguished three arbitrary classes related to the basal ratio of the cochlea including the 0.6 limit used by Churchill et al. [15].

Character states: $\geq$ 0.6, blue; 0.6 > and $\geq$ 0.5, violet; < 0.5, pink.

Character 5: Inter-turn distance

The inter-turn distance is here expressed as a percentage of the width of the basal turn, in order to lessen the effect of size on this variable. Thick walls observed in Odontocetes would enhance acoustical isolation of the hearing organ [17]. Wall thickness has been proposed to characterize high-frequency sensitivity in Odontocetes [11, Figure 7; 17].

Character states: < 7%, blue; 7% ≤ and < 15%, violet; ≤ pink, 15%.

MATRIX

Poebrotherium 01110
Sus 00110
Tayassu 01110
Bos 10021
Ovis 11121
Moschiola 11121
Diacodexis 12?20
Hippopotamus 00010
Choeropsis 00010
Cebochoeridae indet 11120
UMKPGM164 11?01
UMKPGM73 11?11
Basilosauridae 111(10)1
Chaeomysticeti (01)(12)1(01)(01)
Other Odontoceti (12)2(12)(12)(12)
Toothed mysticete 11?11
Echovenator 12121

TREE

(*Poebrotherium*,((*Sus*,*Tayassu*),((*Diacodexis*,(*Moschiola*,(*Bos*,*Ovis*))),((Cebochoeridae,(*Hippopotamus*,*Choeropsis*)),(UMKPGM164,(UMKPGM73,(Basilosauridae,((Chaeomysticeti, Toothed mysticete),(Other Odontoceti, *Echovenator*)))))))));

QUANTIFICATION AND STATISTICAL ANALYSIS

Additional information

The dataset is composed of 64 taxa: 5 archaeocetes, 22 odontocetes (including 8 fossils), 25 mysticetes (including 18 fossils) and 12 land artiodactyls (including 3 fossils), see Data S1 and the KRT in the STAR METHODS section for corresponding references list. The hearing range is known for most of the land artiodactyls [25, 56] and some extant odontocetes [14, 57, 58]. The dataset has been compiled based on the principal component analysis (PCA) of Churchill et al. [15] augmented by the two protocetid specimens from Kpogamé, *Poebrotherium* sp., *Diacodexis ilicis*, one indeterminate cebochoerid and seven extant land artiodactyls. We also added data from the literature: one basilosaurid, 22 mysticetes and three odontocetes from Ekdale and Racicot [11] and Ekdale [18].

PCA was performed on measurements of the cochlea (Data S1) related to hearing physiology [11, 14, 15, 17]. Nine cochlear measurements have been selected, following Fleischer [17], Ekdale and Racicot [11] and Churchill et al. [15]: the cochlear canal length (Cl), the length of the secondary bony lamina (SBL), the number of turn of the cochlear canal (#T), the cochlear height (Ch), cochlear width (Cw), the shorter diameter of the basal turn, perpendicular to Cw (W2), the interturn distance (ITD), the maximal radius of the spiral ganglion canal (GAN) and the area of the fenestra cochlearis (FC). Measurements used in PCA are provided in Data S1. Missing data (10.76% of the dataset) have been estimated using the R package "missMDA" [50] with the cross-validation method ("Kfold"; number of simulation = 10,000). Outliers has been searched with the Grubbs' test [59] using the R package "outliers" [51]. To perform the PCA, we ranked the dataset in order to use the Spearman method, more appropriate than the Pearson method to deal with measurements [60]. The Mahalanobis distance [61] have been calculated on the 5 first PCs. All analyses have been performed with R version 3.3.0 [48].

Script for the analyses performed with R

```
## DATA
  ## Estimating missing data - missMDA
  ## Ranked dataset
  ## PCA - Spearman Method
  ## MAHALANOBIS and Euclidean distances
  ################################## DATA ##################################
  tb<-read.csv2("SI_Dataset_IE.csv",h=T,dec=",",sep="\t",na.string=c("NA"),row.names=1)
  # the dataset is available in Data S1.
  Names<-rownames(tb)
```

```
Cat<-tb[,10]
Cat2<-tb[,11]
Cat3<-tb[,12]
## Missing data
miss<-sum(is.na(tb[,1:9])) # number of ″NA″
nobs<-nrow(tb)
nvar<-ncol(tb[,1:9])
permiss<-round(miss*100/(nobs*nvar),2)
resMiss<-c(miss,permiss)
resMiss
###################### Estimating missing data - missMDA ######################
library(missMDA)
nb<-estim_ncpPCA(tb[,1:9],ncp.min=0,ncp.max=5,method.cv=″Kfold″,nbsim = 10000)
XX<-nb$ncp
res.impute<-imputePCA(tb[,1:9], ncp=XX)
res.impute$completeObs
tb2<-data.frame(Names,res.impute$completeObs,Cat,Cat2,Cat3,row.names=1)
################################ Ranked dataset ################################
rkCl<-rank(tb2[,1])
rkSBL<-rank(tb2[,2])
rkCw<-rank(tb2[,3])
rkCh<-rank(tb2[,4])
rkW2<-rank(tb2[,5])
rkITD<-rank(tb2[,6])
rkGAN<-rank(tb2[,7])
rkFC<-rank(tb2[,8])
rkTurn<-rank(tb2[,9])
tborder<-data.frame(Names,rkCl,rkSBL,rkCw,rkCh,rkW2,rkITD,rkGAN,rkFC,rkTurn,Cat,Cat2,Cat3,row.names=1)
############################ PCA - Spearman Method ############################
library(FactoMineR)
library(factoextra)
res.pcasp=PCA(tborder,scale.unit=TRUE,ncp=5,quali.sup=10:12, graph=T)
summary(res.pcasp)
fviz_pca_ind(res.pcasp, axes=c(1, 2), choix=″ind″, habillage=10)
#################### MAHALANOBIS and Euclidean distances ####################
# Coordinate of the main centroids and the two protocetids on the 5 first PCs
coctr<-res.pcasp$quali.sup$coord
ctrAr<-c(coctr [1,1],coctr [1,2],coctr [1,3],coctr [1,4],coctr [1,5]) # Archaeoceti
ctrLA<-c(coctr [2,1],coctr [2,2],coctr [2,3],coctr [2,4],coctr [2,5]) # Land Artio
ctrMy<-c(coctr [3,1],coctr [3,2],coctr [3,3],coctr [3,4],coctr [3,5]) # Mysticeti
ctrOd<-c(coctr [4,1],coctr [4,2],coctr [4,3],coctr [4,4],coctr [4,5]) # Odontoceti
ctrBa<-c(coctr [8,1],coctr [8,2],coctr [8,3],coctr [8,4],coctr [8,5]) # Basilosauridae
ctrPro<-c(coctr [7,1],coctr [7,2],coctr [7,3],coctr [7,4],coctr [7,5]) # Protocetidae
ctrPel<-c(coctr [6,1],coctr [6,2],coctr [6,3],coctr [6,4],coctr [6,5]) # Pelagiceti
coind<-res.pcasp$ind$coord
(S<-cov(coind))
CoNames<-rownames(coind)
coind2<-data.frame(coind,CoNames)
coind2[coind2[,6]==″Pr_in″,1:5]
Origine5<-c(0,0,0,0,0)
CoGam<-as.numeric(coind2[coind2[,6]==″Pr_in″,1:5])
Gam<-c(CoGam [1],CoGam [2],CoGam [3],CoGam [4],CoGam [5])
CoCar<-as.numeric(coind2[coind2[,6]==″Ca_sp″,1:5])
Car<-c(CoCar [1],CoCar [2],CoCar [3],CoCar [4],CoCar [5])
# Mahalanobis distances
OO<-mahalanobis(Origine5, Origine5, S)
OCar<-mahalanobis(Origine5,Car, S)
OGam<-mahalanobis(Origine5,Gam,S)
OPr<-mahalanobis(Origine5, ctrPro, S)
```

```
OBa<-mahalanobis(Origine5, ctrBa, S)
OAr<-mahalanobis(Origine5, ctrAr, S)
OMy<-mahalanobis(Origine5, ctrMy, S)
OOd<-mahalanobis(Origine5, ctrOd, S)
OPel<-mahalanobis(Origine5, ctrPel, S)
OLA<-mahalanobis(Origine5, ctrLA, S)
resOO<-c(OO,OCar,OGam,OPr,OBa,OAr,OMy,OOd,OPel,OLA)
CarO<-mahalanobis(Car, Origine5, S)
CarCar<-mahalanobis(Car,Car, S)
CarGam<-mahalanobis(Car,Gam,S)
CarPr<-mahalanobis(Car, ctrPro, S)
CarBa<-mahalanobis(Car, ctrBa, S)
CarAr<-mahalanobis(Car, ctrAr, S)
CarMy<-mahalanobis(Car, ctrMy, S)
CarOd<-mahalanobis(Car, ctrOd, S)
CarPel<-mahalanobis(Car, ctrPel, S)
CarLA<-mahalanobis(Car, ctrLA, S)
resCarCar<-c(CarO,CarCar,CarGam,CarPr,CarBa,CarAr,CarMy,CarOd,CarPel,CarLA)
GamO<-mahalanobis(Gam, Origine5, S)
GamCar<-mahalanobis(Gam,Car, S)
GamGam<-mahalanobis(Gam,Gam,S)
GamPr<-mahalanobis(Gam, ctrPro, S)
GamBa<-mahalanobis(Gam, ctrBa, S)
GamAr<-mahalanobis(Gam, ctrAr, S)
GamMy<-mahalanobis(Gam, ctrMy, S)
GamOd<-mahalanobis(Gam, ctrOd, S)
GamPel<-mahalanobis(Gam, ctrPel, S)
GamLA<-mahalanobis(Gam, ctrLA, S)
resGamGam<-c(GamO,GamCar,GamGam,GamPr,GamBa,GamAr,GamMy,GamOd,GamPel,GamLA)
PrO<-mahalanobis(ctrPro, Origine5, S)
PrCar<-mahalanobis(ctrPro,Car, S)
PrGam<-mahalanobis(ctrPro,Gam,S)
PrPr<-mahalanobis(ctrPro, ctrPro, S)
PrBa<-mahalanobis(ctrPro, ctrBa, S)
PrAr<-mahalanobis(ctrPro, ctrAr, S)
PrMy<-mahalanobis(ctrPro, ctrMy, S)
PrOd<-mahalanobis(ctrPro, ctrOd, S)
PrPel<-mahalanobis(ctrPro, ctrPel, S)
PrLA<-mahalanobis(ctrPro, ctrLA, S)
resPrPr<-c(PrO,PrCar,PrGam,PrPr,PrBa,PrAr,PrMy,PrOd,PrPel,PrLA)
BaO<-mahalanobis(ctrBa, Origine5, S)
BaCar<-mahalanobis(ctrBa,Car, S)
BaGam<-mahalanobis(ctrBa,Gam,S)
BaPr<-mahalanobis(ctrBa, ctrPro, S)
BaBa<-mahalanobis(ctrBa, ctrBa, S)
BaAr<-mahalanobis(ctrBa, ctrAr, S)
BaMy<-mahalanobis(ctrBa, ctrMy, S)
BaOd<-mahalanobis(ctrBa, ctrOd, S)
BaPel<-mahalanobis(ctrBa, ctrPel, S)
BaLA<-mahalanobis(ctrBa, ctrLA, S)
resBaBa<-c(BaO,BaCar,BaGam,BaPr,BaBa,BaAr,BaMy,BaOd,BaPel,BaLA)
ArO<-mahalanobis(ctrAr, Origine5, S)
ArCar<-mahalanobis(ctrAr,Car, S)
ArGam<-mahalanobis(ctrAr,Gam,S)
ArPr<-mahalanobis(ctrAr, ctrPro, S)
ArBa<-mahalanobis(ctrAr, ctrBa, S)
ArAr<-mahalanobis(ctrAr, ctrAr, S)
ArMy<-mahalanobis(ctrAr, ctrMy, S)
ArOd<-mahalanobis(ctrAr, ctrOd, S)
```

```
ArPel<-mahalanobis(ctrAr, ctrPel, S)
ArLA<-mahalanobis(ctrAr, ctrLA, S)
resArAr<-c(ArO,ArCar,ArGam,ArPr,ArBa,ArAr,ArMy,ArOd,ArPel,ArLA)
MyO<-mahalanobis(ctrMy, Origine5, S)
MyCar<-mahalanobis(ctrMy,Car, S)
MyGam<-mahalanobis(ctrMy,Gam,S)
MyPr<-mahalanobis(ctrMy, ctrPro, S)
MyBa<-mahalanobis(ctrMy, ctrBa, S)
MyAr<-mahalanobis(ctrMy, ctrAr, S)
MyMy<-mahalanobis(ctrMy, ctrMy, S)
MyOd<-mahalanobis(ctrMy, ctrOd, S)
MyPel<-mahalanobis(ctrMy, ctrPel, S)
MyLA<-mahalanobis(ctrMy, ctrLA, S)
resMyMy<-c(MyO,MyCar,MyGam,MyPr,MyBa,MyAr,MyMy,MyOd,MyPel,MyLA)
OdO<-mahalanobis(ctrOd, Origine5, S)
OdCar<-mahalanobis(ctrOd,Car, S)
OdGam<-mahalanobis(ctrOd,Gam,S)
OdPr<-mahalanobis(ctrOd, ctrPro, S)
OdBa<-mahalanobis(ctrOd, ctrBa, S)
OdAr<-mahalanobis(ctrOd, ctrAr, S)
OdMy<-mahalanobis(ctrOd, ctrMy, S)
OdOd<-mahalanobis(ctrOd, ctrOd, S)
OdPel<-mahalanobis(ctrOd, ctrPel, S)
OdLA<-mahalanobis(ctrOd, ctrLA, S)
resOdOd<-c(OdO,OdCar,OdGam,OdPr,OdBa,OdAr,OdMy,OdOd,OdPel,OdLA)
PelO<-mahalanobis(ctrPel, Origine5, S)
PelCar<-mahalanobis(ctrPel,Car, S)
PelGam<-mahalanobis(ctrPel,Gam,S)
PelPr<-mahalanobis(ctrPel, ctrPro, S)
PelBa<-mahalanobis(ctrPel, ctrBa, S)
PelAr<-mahalanobis(ctrPel, ctrAr, S)
PelMy<-mahalanobis(ctrPel, ctrMy, S)
PelOd<-mahalanobis(ctrPel, ctrOd, S)
PelPel<-mahalanobis(ctrPel, ctrPel, S)
PelLA<-mahalanobis(ctrPel, ctrLA, S)
resPelPel<-c(PelO,PelCar,PelGam,PelPr,PelBa,PelAr,PelMy,PelOd,PelPel,PelLA)
LAO<-mahalanobis(ctrLA, Origine5, S)
LACar<-mahalanobis(ctrLA,Car, S)
LAGam<-mahalanobis(ctrLA,Gam,S)
LAPr<-mahalanobis(ctrLA, ctrPro, S)
LABa<-mahalanobis(ctrLA, ctrBa, S)
LAAr<-mahalanobis(ctrLA, ctrAr, S)
LAMy<-mahalanobis(ctrLA, ctrMy, S)
LAOd<-mahalanobis(ctrLA, ctrOd, S)
LAPel<-mahalanobis(ctrLA, ctrPel, S)
LALA<-mahalanobis(ctrLA, ctrLA, S)
resLALA<-c(LAO,LACar,LAGam,LAPr,LABa,LAAr,LAMy,LAOd,LAPel,LALA)
ResMAL<-data.frame(resOO,resCarCar,resGamGam,resPrPr,resBaBa,resArAr,resMyMy,resOdOd,resPelPel,resLALA)
ResMAL
# Euclidean distance
dist1= Gam [1]-Car [1]
dist2= Gam [2]-Car [2]
dist3= Gam [3]-Car [3]
ResDist=c(abs(dist1),abs(dist2),abs(dist3))
PCs<-c(″PC1″,″PC2″,″PC3″)
ResDist<-data.frame(PCs,ResDist)
ResDist
##############################################################################
```

Detailed description of the PCA results

Outliers

Several variables (Cw, ITD, GAN and FC) present outliers and a total of three different outliers have been found (*Physeter macrocephalus*, the Balaenopteridae TMM 42958-35 and *Eubalaena australis*) for the whole dataset. The presence of these three outliers in the analysis does not impact the result of the PCA.

PCA

The first factorial plane explains 86.58% of the total variation (Figure 2 and Data S2). On PC1 (59.45% of the variance), the main positive contributions come from W2 (contribution (ctr) = 17.67%) along with Cw (ctr = 16.55%), Cl (ctr = 14.70%), and Ch (ctr = 13.61%). The only negative contribution on PC1 is weak and comes from #T (ctr < 1%). PC2 (27.13% of the variance), opposes the positive contributions of the variables #T (ctr = 33.61%) and FC (ctr = 11.52%) with the negatives ones of the variables ITD (ctr = 17.39%), GAN (ctr = 13.76%) and SBL (ctr = 10.75%).

On PC1, the two protocetids from Kpogamé are distant with a Euclidean distance (Ed) of 0.18. Yet, protocetid indeterminate γ differs from ?*Carolinacetus* sp. by having wider cochlea (W2 = 7.0 versus 5.8) and a shorter cochlear canal (Cl = 22.44 versus 28.07). The main differences between them are enlighten on PC2 (Ed = 1.21) with a smaller secondary bony lamina for protocetid indeterminate γ (SBL = 8.9 versus 10.4), smaller fenestra cochlearis (FC = 4.80 versus 8.55) and a higher interturn distance (ITD = 1.2 versus 0.9). The Mahalanobis distance (Md; see Data S2) between the centroids of protocetids and land artiodactyls is 2.48 while it is 3.46 between protocetids and Pelagiceti. Yet, protocetids includes only two specimens. In details, ?*Carolinacetus* sp. is closer to the centroid of land artiodactyls (Md = 1.69) than the one of Mysticeti (Md = 4.33) and of Odontoceti (Md = 5.17), while the protocetid indeterminate γ is closer to that of Odontoceti (Md = 4.25) than that of land artiodactyls (Md = 4.08) and of Mysticeti (Md = 6.69).

The basilosaurid morphospace overlaps that of early mysticetes (cyan squares on Figure 2) and is included within the Mysticeti morphospace. The centroid of the former is closer to that of Mysticeti (Md = 2.42) than to that of land artiodactyls (Md = 3.10) or to that of Odontoceti (Md = 3.48). Yet, the centroid of Archaeoceti remains closer to that of land artiodactyls (Md = 2.60) than to that of Mysticeti (Md = 3.24) and Odontoceti (Md = 3.56).

DATA AND SOFTWARE AVAILABILITY

The datasets used for the PCA and for the reconstruction of ancestral character states (character state discretization) are available in this paper (Data S1).

The 3D model of the bony labyrinth of UM-KPG-M 164 referred to ?*Carolinacetus* sp. is available at http://MorphoMuseuM.com under the number M3#149_UMKPG-M164 (http://dx.doi.org/10.18563/m3.3.2.e4).

The 3D model of the bony labyrinth of UM-KPG-M 73 referred to Protocetidae indeterminate (morphotype γ) is available at http://MorphoMuseuM.com under the number M3#150_UMKPG-M73 (http://dx.doi.org/10.18563/m3.3.2.e4).

Current Biology, Volume *27*

Supplemental Information

Infrasonic and Ultrasonic Hearing Evolved after the Emergence of Modern Whales

Mickaël J. Mourlam and Maeva J. Orliac

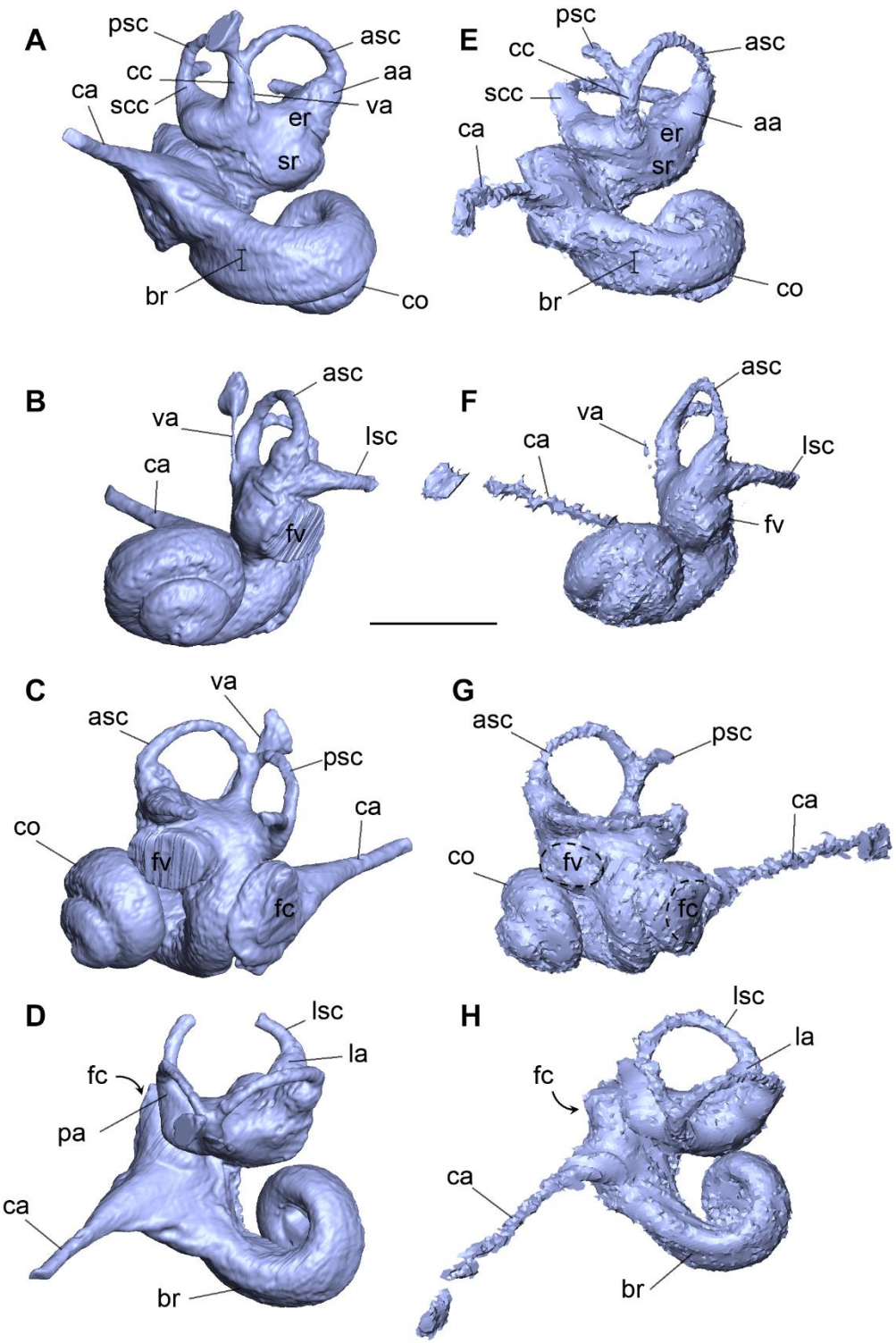

Figure S1.
3D models of the casts of the bony labyrinths of ?*Carolinacetus* sp. (UM-KPG-M 164; A-D) and of the protocetid indeterminate (morphotype γ; UM-KPG-M 73; E-H) from Kpogamé illustrated in medial (A, E), anterior (B, F), lateral (C, G), dorsal (D, H) views. Related to Figure 1. Scale bar = 5 mm. Abbreviations: **aa**, anterior ampulla; **asc**, anterior semicircular canal; **br**, basal ridge (imprint); **ca**, cochlear aqueduct; **cc**, common crus; **co**, cochlear canal; **er**, elliptical recess; **fc**, fenestra cochleae; **fv**, fenestra vestibuli; **la**, lateral ampulla; **lsc**, lateral semicircular canal; **pa**, posterior ampulla; **psc**, posterior semicircular canal; **scc**, secondary common crus; **sr**, spherical recess; **va**, vestibular aqueduct.

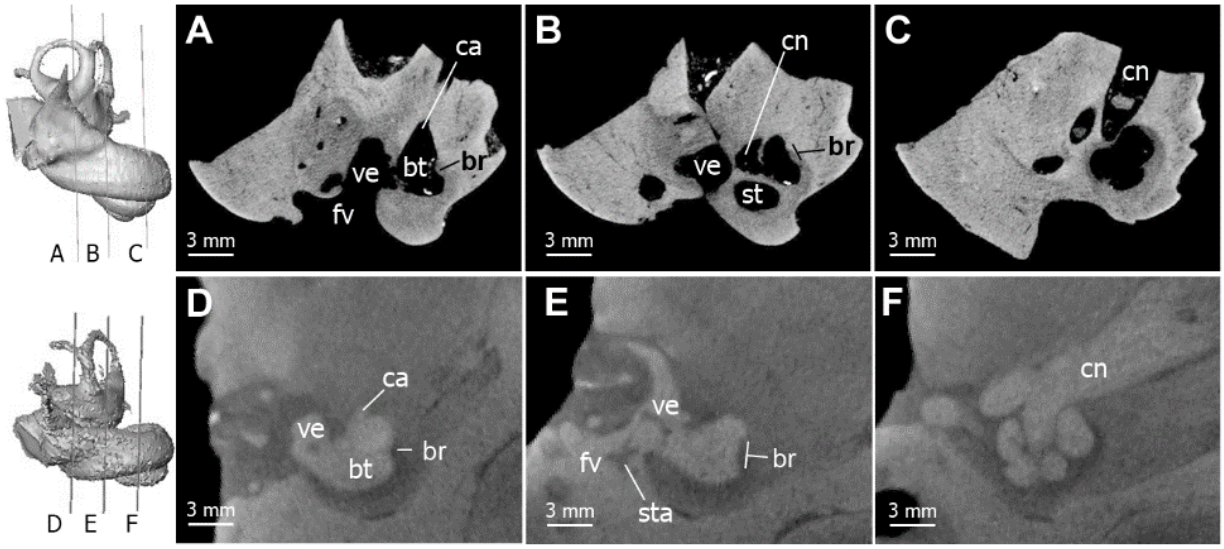

Figure S2.
Cross sections through the bony labyrinths of ?*Carolinacetus* sp. UM-KPG-M 164 (A-C) and of the protocetid indeterminate γ UM-KPG-M 73 (D-F). Related to Figure 1. Abbreviations: **br**, basal ridge; **bt**, basal turn; **ca**, cochlear aqueduct; **cn**, cochlear nerve canal; **fv**, fenestra vestibuli; **st**, second turn; **sta**, stapes; **ve**, vestibule.

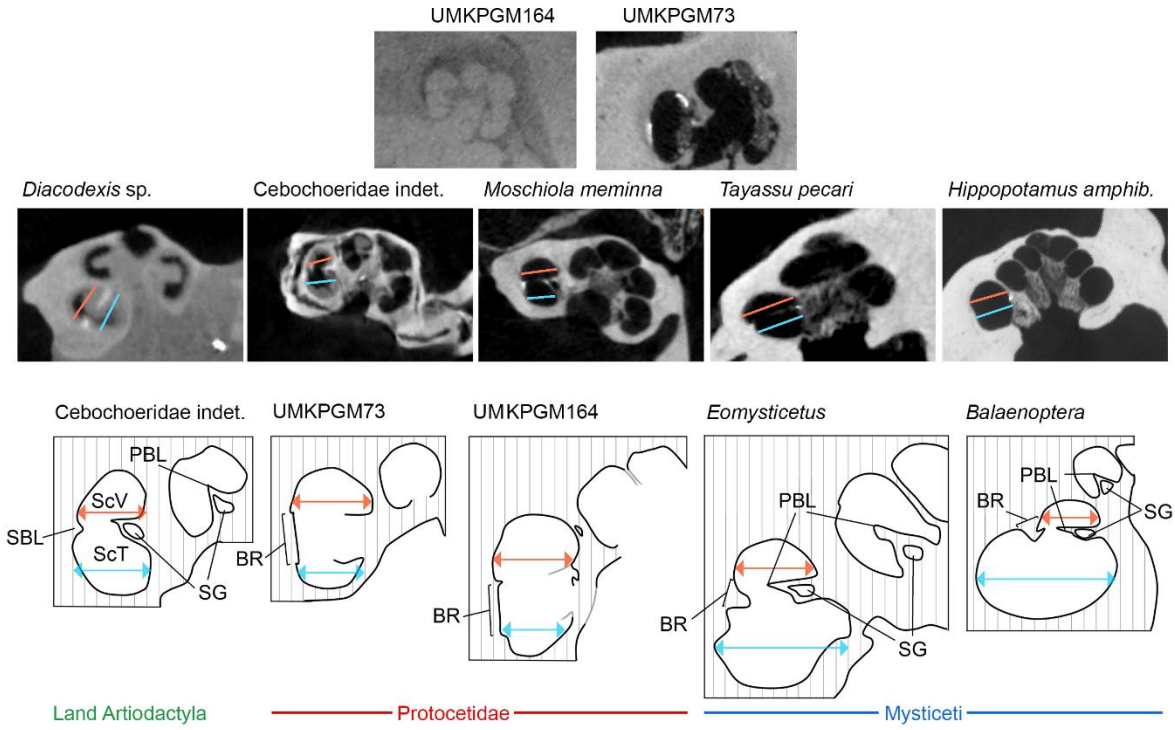

Figure S3.
Cross sections at ¼ turn through the cochlear canal of land artiodactyls, protocetids and mysticetes. **Related to Figure 1.** Specimen's numbers are the same as in Table S2. Orange arrows and lines are indicative of Scala vestibuli width, blue arrows and lines are indicative of Scala tympani width. The contrast of the primary and secondary bony laminae has been artificially increased. Simplified block diagram of *Eomysticetus* drawn after Ekdale [S1, fig. 4E], that of *Balaenoptera* after Fleischer [S2, fig. 7]. Abbreviations: **BR**, basal ridge; **PBL**, primary bony lamina; **SBL**, secondary bony lamina; **ScV**, Scala vestibuli; **ScT**, Scala tympani; **SG**, spiral ganglion.

	?Carolinacetus sp. UM-KPG-M164	Protocetid indet. UM-KPG-M73
Labyrinth volume	179.22	116.76
Cochlea volume	131.93	81.25
Vestibule volume	47.29	35.51
Cochlea vol/Vol tot	73.61	69.59
Cochlear coil (°)	810	765
Number of turns	2.25	2.10
Cochlea height	4.82	4.85
Basal turn width	9.24	8.81
Cochlear canal length	28.07	22.44
SBL length	10.40	8.90
SBL coil	180	180
Axial pitch	2.33	2.76
Basal ratio of cochlea	0.62	0.56
Cochlear slope	0.075	0.103
R A	1.80	1.79
R L	2.10*	1.88
R P	1.40	1.44*
L A	7.35	7.7
L L	8.28*	6.68
L P	7.13	6.48*
θAL	80	88
θAP	95	99
θPL	87	91

Table S1. Measurements of the bony labyrinth endocast of Protocetid whales from Kpogamé. Related to Figure 1.

Length and width expressed in mm, Volumes expressed in mm3; Height of cochlear canal and width of the basal turn measured following Ekdale and Rowe [S3]; axial pitch and basal (aspect) ratio of cochlea, and cochlear slope calculated following Ekdale and Racicot [S4]. The semicircular canal radius (R) corresponds to the quarter of the sum of the height (h) and the width (w) of the semicircular canal (*i.e.* R = (h + w)/4), following Spoor and Zonneveld [S5]. Angles between the planes of the semicircular canals were measured following Ekdale [S6: 1900]. **Cochlea vol/Vol tot** corresponds to the contribution in percentage of the cochlea to the total volume of the bony labyrinth; the cochlea volume includes the cochlear aqueduct. **R A**, Canal radius of the ASC (mm); **R L**, Canal radius of the LSC (mm); **R P**, Canal radius of the PSC (mm); **L A**, Length of the ASC (mm); **LL**, Length of the LSC (mm); **LP**, Length of the PSC (mm); **θAL**, Angle between the ASC and LSC; **θAP**, Angle between the ASC and PSC; **θPL**, Angle between the PSC and LSC. * estimated values.

Data S1. List of taxa and measurments included in the PCA and in ancestral character state reconstruction. Related to Figures 2 and 3. See spreadsheet.
List of taxa included in the PCA (illustrated in Figure 2) with corresponding specimen number, abbreviation, reference, cochlear measurements and ratios used in the PCA (in grey) and in ancestral character state reconstruction (illustrated in Figure 3; colour code of the last 5 columns corresponds to the character state attribution). The first eight parameters correspond to those used by Churchill *et al.* [S7]; we added the number of turns as a ninth character. Abbreviations: (**Ch**) cochlear height, (**Cl**) cochlear canal length, (**Cw**) cochlear width, (**FC**) area of the fenestra cochlearis, (**GAN**) maximal radius of the spiral ganglion canal, (**ITD**) inter-turn distance, (**SBL**) length of the secondary bony lamina, (**W2**) shorter diameter of the basal turn, perpendicular to Cw, (**#T**) number of turn of the cochlear canal, (**%GAN**) diameter of the spiral ganglion expressed as a percentage of the area of the fenestra cochlearis [S7], (**%ITD**) inter-turn distance expressed as a percentage of the width of the basal turn [S7], (**%SBL**) extension of the SBL expressed as a percentage of the cochlear canal length. **NA**, indicates for non-available data. **cat**, **cat2**, **cat3**, refer to the different categories used in the PCA (see script for the statistical analyses). Abbreviations of museum collections: **AMNH**, American Museum of Natural History, New York City USA; **CAS**, California Academy of Sciences, San Francisco USA; **CCNHM**, Mace Brown Natural History Museum, Charleston USA; **ChM**, Charleston Museum, Charleston USA; **CMM**, Calvert Marine Museum, Solomons USA; **GSM**, Georgia Southern Museum, Statesboro USA; **HSU**, Natural History Museum, Humboldt State University, Arcata USA; **IPHEP**, Institute of Paleoprimatology, Human Paleontology: Evolution and Paleoenvironments, Poitiers France; **LACM**, Natural History Museum Los Angeles County, Los Angeles USA; **MNHN**, National Museum of Natural History, Paris France; **SDNHM/SDSNH**, San Diego Museum Natural History Museum, San Diego USA; **TMM**, Texas Natural Science Center, Austin USA; **UM**, University of Montpellier, Montpellier France; **UO**, Museum of Natural and Cultural History, University of Oregon, Eugene USA; **USNM**, National Museum of Natural History, Washington D.C.

Data S2. Statistical supplements. Related to Figure 2. See spreadsheet.
Contains the summary of the PCA and the Mahalanobis distances between the main groups and the two protocetids from Kpogamé. Additional information and script are provided in the STAR METHOD.

Supplemental References

S1. Ekdale, E.G. (2016). Morphological variation among the inner ears of extinct and extant baleen whales (Cetacea: Mysticeti). J. Morphol. *277*, 1599–1615.
S2. Fleischer, G. (1976). Hearing in Extinct Cetaceans as Determined by Cochlear Structure. J. Paleontol. *50*, 133–152.
S3. Ekdale, E.G., and Rowe, T. (2011). Morphology and variation within the bony labyrinth of zhelestids (Mammalia, Eutheria) and other therian mammals. J. Vertebr. Paleontol. *31*, 658–675.
S4. Ekdale, E.G., and Racicot, R.A. (2015). Anatomical evidence for low frequency sensitivity in an archaeocete whale: Comparison of the inner ear of *Zygorhiza kochii* with that of crown Mysticeti. J. Anat. *226*, 22–39.
S5. Spoor, F., and Zonneveld, F. (1998). Comparative review of the human bony labyrinth. Am. J. Phys. Anthropol. *Suppl 27*, 211–251.
S6. Ekdale, E.G. (2010). Ontogenetic Variation in the Bony Labyrinth of *Monodelphis domestica* (Mammalia: Marsupialia) Following Ossification of the Inner Ear Cavities. Anat. Rec. *293*, 1896–1912.
S7. Churchill, M., Martinez-Caceres, M., de Muizon, C., Mnieckowski, J., and Geisler, J.H. (2016). The Origin of High-Frequency Hearing in Whales. Curr. Biol. *26*, 2144–2149.
S8. Orliac, M.J., Benoit, J., and O'Leary, M.A. (2012). The inner ear of Diacodexis, the oldest artiodactyl mammal. J. Anat. 221, 417–426.